JGR Solid Earth

RESEARCH ARTICLE
10.1029/2024JB030641

Interseismic Megathrust Coupling at the Osa Peninsula, Costa Rica

Mason Perry[1], **Cyril Muller**[2], **Marino Protti**[2], **Lujia Feng**[1,3], **and Emma M. Hill**[1,3]

[1]Earth Observatory of Singapore, Nanyang Technological University, Singapore, Singapore, [2]Observatorio Vulcanolóogico y Sismológico de Costa Rica, Heredia, Costa Rica, [3]Asian School of the Environment, Nanyang Technological University, Singapore, Singapore

Key Points:

- The Osa Peninsula has been subject to large (magnitude > 7) earthquakes every ∼40 years, most recently in the 1983 magnitude 7.4 event
- A new geodetic coupling model indicates the region of the 1983 rupture has accumulated enough strain to host a similar magnitude event
- Slow slip events reduce the overall coupling in localized patches and may influence spatial patterns of a future rupture

Supporting Information:

Supporting Information may be found in the online version of this article.

Correspondence to:

M. Perry,
masonkyle.perry@ntu.edu.sg

Citation:

Perry, M., Muller, C., Protti, M., Feng, L., & Hill, E. M. (2025). Interseismic megathrust coupling at the Osa Peninsula, Costa Rica. *Journal of Geophysical Research: Solid Earth*, *130*, e2024JB030641. https://doi.org/10.1029/2024JB030641

Received 3 NOV 2024
Accepted 21 JUN 2025
Corrected 4 AUG 2025

This article was corrected on 4 AUG 2025. See the end of the full text for details.

Author Contributions:

Conceptualization: Mason Perry, Cyril Muller, Marino Protti, Lujia Feng, Emma M. Hill
Data curation: Mason Perry, Cyril Muller, Marino Protti
Formal analysis: Mason Perry, Cyril Muller
Funding acquisition: Marino Protti, Lujia Feng, Emma M. Hill
Investigation: Mason Perry, Cyril Muller, Marino Protti, Lujia Feng
Methodology: Mason Perry, Cyril Muller, Marino Protti, Lujia Feng, Emma M. Hill

Abstract At the Osa Peninsula in southern Costa Rica, magnitude >7 earthquakes have been generated along the Middle American trench in 1904, 1941, and 1983 following a ∼40-year recurrence interval, suggesting a rupture may be impending. However, regional interseismic coupling remains poorly constrained, largely due to sparse observations that are likely contaminated by aliasing effects of repeating shallow slow slip events (SSEs) that occur roughly every 4 years, but were only discovered recently. These SSEs, while likely reducing megathrust coupling near the trench, may load or trigger the next rupture of the 1983 asperity. Using new continuous Global Navigation Satellite System (GNSS) data from an updated and densified regional network, we derive inter-SSE rates of deformation and invert for slip deficit and megathrust coupling along the Middle American Trench, implementing block modeling to correct for the motion of the Panama microplate. We invert for slow slip and remove a time-averaged estimate of cumulative slow slip from our models. Our results indicate that the region of highest inter-SSE coupling (>0.8) corresponds with the spatial extent of SSE slip. We also find that SSEs are sufficient to release nearly all the elastic strain accumulated over their 4-year recurrence interval in localized regions. Accounting for this, in the region immediately downdip of the slow slip patch—the same region thought to have ruptured in the 1983 M_w 7.4 event—we estimate an interseismic coupling ratio of ∼0.5–0.7 corresponding to ∼1.75–2 m of accumulated slip deficit since 1983, sufficient to generate a similar magnitude rupture in the future.

Plain Language Summary Megathrust coupling at the Osa Peninsula of Costa Rica has historically been poorly constrained due to sparse observations, but accurate coupling estimates are vital for understanding and forecasting seismic hazard in the region. The megathrust offshore southern Costa Rica has been host to a number of historical earthquakes, generating magnitude >7 events in 1904, 1941, and most recently 1983, following a ∼40-year recurrence interval. This pattern of earthquakes suggests a rupture may be impending, emphasizing the urgent importance of understanding the location and behavior of frictionally locked asperities on the megathrust. In this paper we present new estimates of coupling based on data from an updated and densified regional geodetic observation network. We also account for the influence of slow slip events (effectively slow earthquake ruptures) on estimates of megathrust coupling. Overall, we find that enough strain has accumulated on the megathrust at the Osa Peninsula to generate an earthquake as large as the 1983 M_w 7.4 event.

1. Introduction

Many of the largest earthquakes experienced on the Osa Peninsula of southern Costa Rica result from frictional locking on the interface between the rapidly subducting Cocos plate and the overriding Panama microplate (e.g., Adamek et al., 1988; Kellogg et al., 1995). Regional historic seismicity includes at least three $M > 7$ events, with the most recent being the 3 April 1983 M_w 7.4 event (e.g., Adamek et al., 1988; Kellogg et al., 1995). Previous events occurred in 1941 (Ms 7.5), 1904 (Ms 7.6), and probably in 1867 (Protti et al., 2001), following a ∼40-year recurrence interval (Adamek et al., 1987). The estimated epicenters of the two most recent events were located along the coast of the Costa Rican mainland, eastward of the Osa Peninsula (Figure 1a). Estimated slip distributions of the 1983 event include the region to the northwest and west of the estimated focal mechanism (Figure 1a; Adamek et al., 1987; Tajima & Kikuchi, 1995).

In addition to coseismic slip related to megathrust earthquakes, slow slip along the Middle America Trench has been documented in multiple locations. At the Nicoya Peninsula several slow slip events (SSEs) have been

Project administration: Cyril Muller, Marino Protti
Resources: Cyril Muller, Marino Protti, Emma M. Hill
Supervision: Lujia Feng, Emma M. Hill
Validation: Mason Perry
Visualization: Mason Perry
Writing – original draft: Mason Perry, Cyril Muller
Writing – review & editing: Mason Perry, Cyril Muller, Marino Protti, Lujia Feng, Emma M. Hill

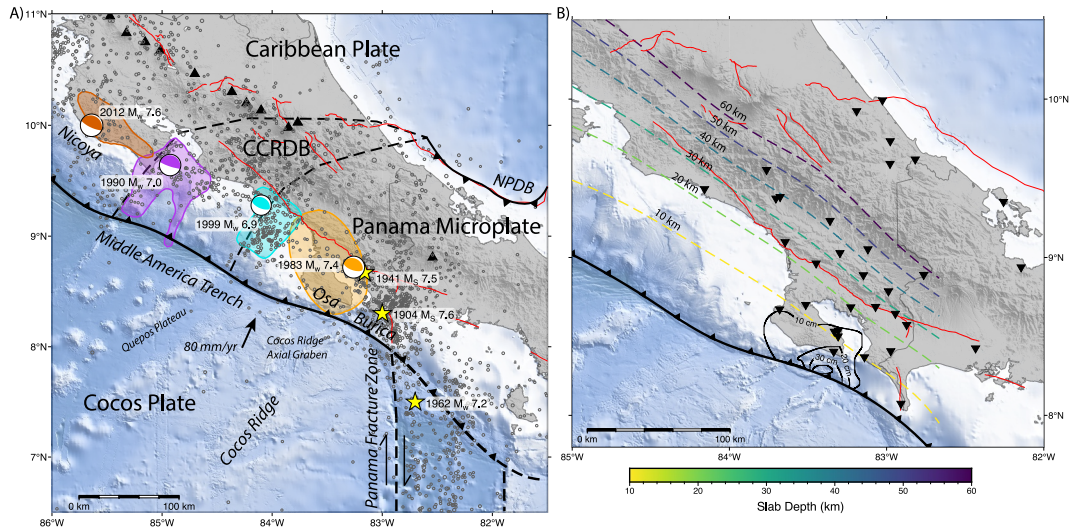

Figure 1. Overview of the Osa Peninsula and surrounding region. Panel (a) shows tectonic boundaries are plotted as black lines, with dashed lines indicating inferred boundaries. NPDB stands for the North Panama Deformed belt, demarking the boundary between the Panama Microplate and the Caribbean Plate. CCRDB stands for Central Costa Rica Deformed Belt, which is a region of diffuse deformation between the western edge of the Panama microplate and the Caribbean plate (e.g., Marshall et al., 2000), and is plotted with the geometry preferred by Carvajal-Soto et al. (2020). Tectonic velocity of the Cocos plate toward the Caribbean plate is from DeMets et al. (2010). Volcanoes are plotted as black triangles, while faults from the Caribbean and Central American active fault database are plotted as red lines (Styron et al., 2020). Recent significant (M_w > 6.5) intraplate earthquakes are plotted with focal mechanisms from the CMT catalog (Dziewonski et al., 1981; Ekström et al., 2012). When focal mechanisms are unconstrained or unknown, epicenters are plotted as yellow stars. The slip region for the 2012 M_w 7.6 Nicoya event if from Hobbs et al. (2017), while the epicenter is taken from the CMT catalog. The slip region and epicenter for the 1990 M_w 7.0 Nicoya Gulf event is taken from Protti et al. (1995). The slip region for the 1999 M_w 6.9 Quepos event is from DeShon et al. (2003) while the epicenter is taken from the CMT catalog. The slip region and epicenter location for the 1983 M_w 7.4 Osa event is taken from Adamek et al. (1987), as are the epicenters for the 5 December 1941 and the 20 December 1904 historical events. Also plotted is the epicenter of the 26 July 1962 M_w 7.2 event on the Panama Fracture Zone, taken from Molnar and Sykes (1969). Background seismicity from the USGS catalog from 1980 to 2024 are plotted as gray circles and sized by magnitude (https://earthquake.usgs.gov/earthquakes/search). Panel (b) shows a zoomed in map of the Osa and Burica Peninsulas with the locations of continuous GNSS stations used in our modeling as inverted triangles. Contours of cumulative slow slip at Osa is also shown with 10 cm intervals, contours are based on offsets from Perry et al. (2023), calculated in this paper (see Section 3). Slab contours are also plotted based on Slab2 (Hayes et al., 2018), and have been shifted to better align with regional seismicity (Figure S4 in Supporting Information S1), and extend to a maximum of 60 km in depth.

observed (e.g., Brown et al., 2005; Davis et al., 2015; Jiang et al., 2012), and seem to play a role in modulating the spatial extent of large ruptures (Dixon et al., 2014; Xie et al., 2020). To the south, at the Osa Peninsula, regular shallow SSEs were recently observed and have magnitudes sufficient to fully account for tectonic convergence in localized regions (Figure 1b; Perry et al., 2023). These events may modulate the spatial distribution of slip in future earthquakes (e.g., Dixon et al., 2014), or potentially play a role in their triggering (e.g., Kato et al., 2012; Uchida et al., 2016).

As we are near the end of a ~40-year recurrence interval, an accurate estimate of coupling in the region is critical. However, existing geodetic estimates of coupling ratios in the region exhibit both notable variation as well as relatively low resolution. Both La Femina et al. (2009) and Kobayashi et al. (2014) found a largely intermediate state of coupling (~0.4–0.6) in southern Costa Rica, while the more recent study of Carvajal-Soto et al. (2020) estimated nearly full coupling (~0.98–1) in the region. However, these estimates include a significant amount of campaign-style surveys with low temporal resolution. Recent densification of the continuous Global Navigation Satellite System (GNSS) network in southern Costa Rica allows us to investigate regional coupling with much denser spatial resolution than these previous studies. Additionally, the discovery of large (M_w ~6.5–6.7) ~3–6 weeks-long shallow SSEs offshore and beneath the Osa Peninsula occurring at a ~4-year recurrence interval (Perry et al., 2023), indicates these prior geodetic observations may have yielded inaccurate estimates of long-term megathrust coupling.

At the Osa Peninsula, we have terrestrial observations that are particularly close to the trench (often <40 km), much closer than is possible for most subduction zones. As such, this region provides a unique opportunity to study shallow subduction zone processes without the need for ocean-bottom observations. Additionally, recent work on the effect of stress shadows on coupling indicates that the coupled regions of megathrusts likely also include regions updip of frictionally locked asperities that are only kinematically coupled (Almeida et al., 2018; Lindsey et al., 2021), and by accounting for realistic stress constraints we can theoretically improve the accuracy of offshore coupling estimates. Thus, the near-trench observations at the Osa Peninsula, provide an opportunity to test the viability of the stress-constrained method.

Here, we present new geodetic velocity estimates using time series from a network of continuous GNSS stations in southern Costa Rica, and we calculate a new coupling model for the region. We also compare results from standard elastic inversions and those using more realistic stress constraints. Lastly, we investigate how SSEs appear to modulate the coupling ratio in southern Costa Rica, highlighting regions that are highly coupled and liable to rupture in future earthquakes.

Throughout this paper, we use multiple terms to refer to related but distinct behavior on the megathrust interface. We use "coupling" to indicate the level to which the megathrust is geodetically estimated to be not slipping. Typically represented as a ratio, a coupling value of 1 indicates the megathrust is not slipping, whereas a coupling ratio of 0 indicates the megathrust is creeping. "Slip deficit" and "slip deficit rate" refer to the difference between the expected slip should the megathrust be slipping in the absence of frictional locking at the plate rate and the slip i.e. estimated geodetically. Lastly, "frictionally locked" refers to frictional behavior on the megathrust, generally asperities, that cause coupling. It is important to note that from geodetic observations we can only infer coupling and slip deficit, not frictional locking, as frictionally locked asperities can influence the state of coupling on surrounding regions (e.g., Lindsey et al., 2021).

2. Tectonic Background

Based on crustal dynamics, Costa Rica is often divided into four primary tectonic regions (e.g., Carvajal-Soto et al., 2020). In the north/northeast of the country, the broadly flat backarc northeast of the volcanic arc is largely considered part of the Caribbean plate, while the northwest coast west of the volcanic arc, includes the Nicoya Peninsula and is often defined as part of the Central American Forearc that extends northward to Guatemala (Iinuma et al., 2004; Kobayashi et al., 2014; Lundgren et al., 1999; Rodriguez et al., 2009). Immediately to the south and east of these is the Central Costa Rica Deformed Belt (CCRDB) that consists of diffuse and complex faulting associated with changes in subducting seafloor roughness from the relatively smooth bathymetry of the north to subducting seamounts further south (e.g., Marshall et al., 2000). Lastly, the remaining portion of Costa Rica is generally ascribed to the Panama microplate (e.g., Adamek et al., 1988; Kellogg et al., 1995), bounded by the North Panama Deformed Belt (NPDB) to the north where the Panama microplate is thrust on top of the Caribbean plate (Adamek et al., 1988), with the boundary variously described as a collisional back-arc fold and thrust belt (e.g., Protti & Schwartz, 1994; Suárez et al., 1995), or a nascent subduction zone (e.g., Camacho et al., 2010).

In southern Costa Rica near the Osa Peninsula, the onshore tectonics are dominated by effects of subduction of the thick and relatively buoyant Cocos ridge. Previous studies found trench-normal tectonic velocities directly landward of the Cocos ridge, with regions to the northwest exhibiting increasingly large westward components due to escape tectonics and a developing forearc sliver, especially further northwest into Nicaragua (Kobayashi et al., 2014; La Femina et al., 2009). To the southeast of the Osa Peninsula, the Panama fracture zone separates the rapidly subducting Cocos plate from the Nazca plate (Molnar & Sykes, 1969; Morell et al., 2008), with the trace of the fracture zone approximately aligning with the Burica Peninsula (Figure 1).

In the regions surrounding the Osa Peninsula, and Costa Rica in general, complex tectonics have produced significant seismicity. To the southeast, relatively large strike-slip events have been recorded offshore southern Costa Rica driven by the differential movement between the Cocos and Nazca plates, including the 1962 M_s 7.3 event (Ambraseys & Adams, 1996; Molnar & Sykes, 1969). To the northwest of the Osa Peninsula, the subduction of the Cocos plate beneath the CCRDB and the influence of subducted bathymetric highs (i.e., former seamounts) has yielded significant seismic activity including the 1999 M_w 6.9 Quepos earthquake (e.g., Bilek et al., 2003; DeShon et al., 2003; Protti et al., 1995). Further north, the Nicoya Peninsula was host to a large M_w 7.6 earthquake in 2012 (e.g., Malservisi et al., 2015; Protti et al., 2014), that was accurately anticipated by models

of coupling on the plate interface (Feng et al., 2012; Protti et al., 2014), and potentially modulated by SSEs in the region (e.g., Dixon et al., 2014; Xie et al., 2020).

3. Methods

3.1. GNSS Data and Processing

As a tool to determine regions that may be more or less prone to future seismic ruptures, coupling inversions have shown promising results in other regions of Costa Rica (e.g., Feng et al., 2012), accurately forecasting regions of eventual seismic slip (Protti et al., 2014). Often calculated using various geodetic observations, accurate coupling models are dependent on observations that both reflect long-term interseismic deformation and limit signals imposed by processes other than frictional locking on the fault of interest. At the Osa Peninsula in southern Costa Rica, in anticipation of potential future megathrust earthquakes, in recent years the Observatorio Vuclcanólogico y Sismológico de Costa Rica (OVSICORI-UNA) has been densifying the regional seismic network and establishing a continuously operating GNSS network in and around the region. Prior to 2017, only eight continuous global GNSS stations were operating in southern Costa Rica, with just one on the Osa Peninsula. Campaign-style GNSS data were collected during four previous campaigns in 2000, 2003, 2007, and 2010. Most sites were only measured two to three times, resulting in sparse spatial and temporal coverage in the reigon. The updated network, along with additional stations operated by the Instituto Geografico Nacional (IGN) (https://gnss.rnp.go.cr/SBC/) and the Insituto Costarricense de Electricidad (ICE), have been recently used to detect shallow SSEs just offshore and underneath the Osa Peninsula (Perry et al., 2023), but have not yet been used to determine megathrust coupling in the region. Notably, we do not use any data from older campaign-style GNSS observations in this study to avoid potential aliasing effects of undetected SSEs on long-term velocity estimates.

We processed the GNSS data from this densified network using the GAMIT/GLOBK software suite (Herring et al., 2015, 2018) following the method described in Perry et al. (2023). Using final orbital products from the International GNSS Service and the Vienna mapping function of Boehm et al. (2006), we corrected for tropospheric delays following the processing approach described in Herring et al. (2016). The network was first tied into the 2014 International Terrestrial Reference Frame (ITRF2014) (Altamimi et al., 2016). We then transformed the resulting position estimates to be relative to the stable Caribbean reference frame by first applying the ITRF2014 to ITRF2008 transformation defined by Altamimi et al. (2016), and then removed the predicted ITRF2008-Caribbean velocity model defined by Altamimi et al. (2012).

3.2. Inter-SSE Velocities and Offset Estimation

In working toward a representative model of interseismic megathrust coupling in southern Costa Rica, we needed to ensure that slip released in SSEs was accurately accounted for in our preferred coupling model. While other studies of coupling in regions of frequent SSEs use long-term velocity estimates over uniform time periods as a way of averaging out the influence of temporally and spatially variable SSEs (e.g., Maubant et al., 2022, 2023), the temporally disjointed nature of observations in our study region, coupled with recent densification of the network makes this difficult to do. Several stations began recording as early as 2010, while others have only been recording since 2021 (Figure S1 in Supporting Information S1). Furthermore, some stations stopped recording for long periods of time during the COVID-19 pandemic, while others have either gone offline or have periods of poor data quality. Additionally, SSEs seem to occur every ∼4 years in the region (Perry et al., 2023), with few time series that span multiple slow slip cycles (Figure 2a). Thus, inconsistent temporal sampling is liable to introduce significant errors in long-term velocity estimates. A rudimentary analysis for one station (PIRO) using different sampling epochs shows up to ∼45% variation in linear velocity estimates (Figure 2b), which could significantly influence the estimated coupling ratio. In order to derive the most accurate estimation of coupling on the megathrust, we base our inverse models of coupling (Section 3.4) on inter-SSE velocities calculated following the approach outlined below. As they are based on inter-SSE velocities, the resulting models will reflect the influence of frictional locking that is released in both seismic ruptures and SSEs, that is, both seismogenic and slow-slip asperities. Finally, to account for the influence of the SSEs on the overall state of coupling, we then model SSE slip and estimate the degree to which it reduces the overall slip deficit (Section 3.4), and remove it from our coupling model yielding a more representative interpretation of regional coupling.

Inter-SSE velocities were calculated from daily position time series spanning from 2016 to 2024 for 33 regional GNSS stations (Figure 3a). Following Perry et al. (2023), we removed outliers from the daily time series, defined

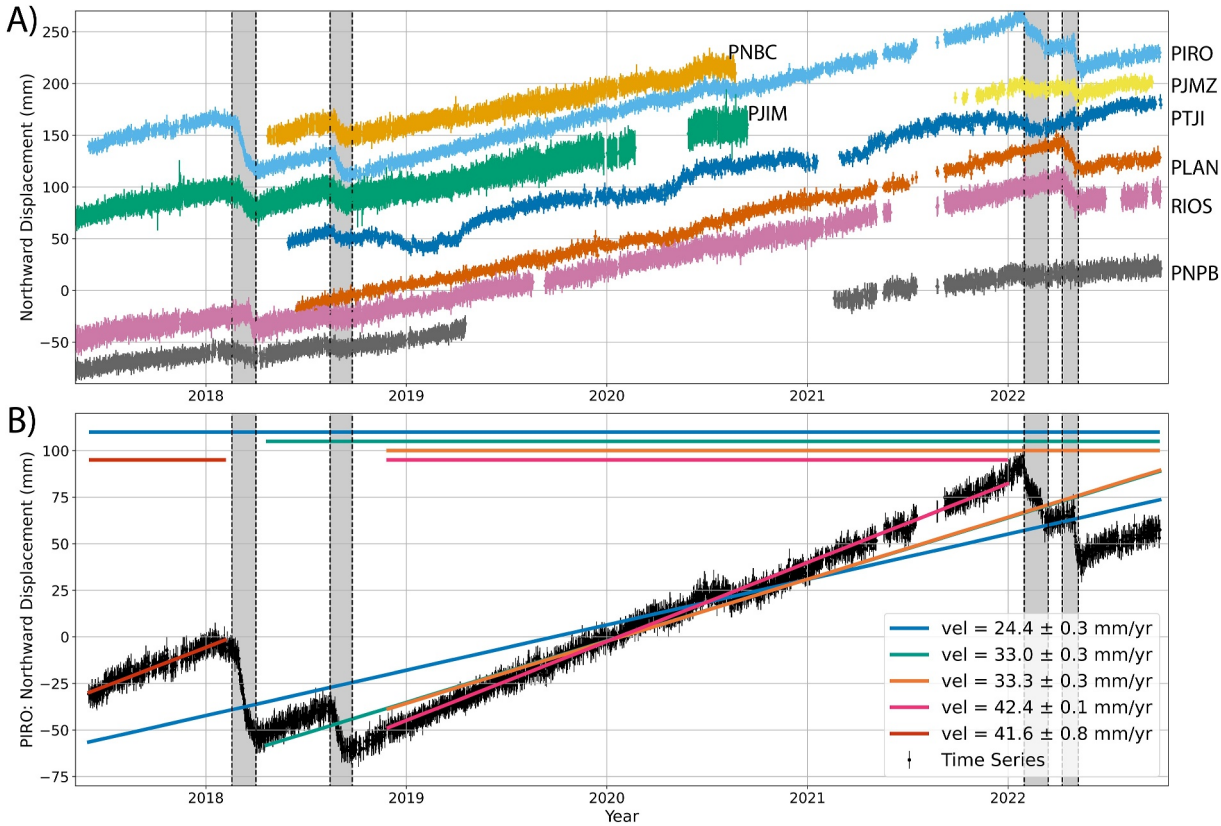

Figure 2. Selected GNSS time series plots to illustrate the temporally disjointed network and justify our use of inter-SSE rates for coupling models. Timing of SSEs is indicated by the shaded regions. Panel (a) shows the north component of time series of stations that recorded SSEs in 2018 and 2022. Some stations (e.g., PIRO, RIOS) were recording during all four SSEs, while some (e.g., PNBC) were only recording during one SSE. Such observations preclude the use of any single uniform time period to determine long-term interseismic velocities. Panel (b) shows the time series of an example station (PIRO), and a range of linear rates derived using different observational periods with 1σ errors. For the north component, the velocity variation can be up to ~50% for this example station. If such variations were propagated into inversions, significant bias would be introduced into the models. Inter-SSE rates appear to exhibit little variation before or after SSEs.

as position estimates with formal errors larger than two standard deviations of the mean position error. We also removed non-tidal atmospheric loading using estimates from the models calculated by Dill and Dobslaw (2013). The resulting time series were then cross referenced with the regional earthquake catalog from the USGS (https://earthquake.usgs.gov/earthquakes/search), and coseismic and instrumental offsets were removed where apparent. The entire data set includes both coseismic and postseismic offsets from two relatively large events (the 2012 M_w 7.6 Nicoya event and a 2017 M_w 6.5 event centered near Jacó, Costa Rica) as well as some signals likely related to smaller events (a 2018 M_w 6.1 event centered near the Osa Peninsula, Costa Rica; a series of four M_w 4.7–5.7 events on 29 January 2021 centered near the Burica Peninsula; and two M_w 6–6.2 strike-slip events on 13 May and 26 June 2019 respectively also centered near the Burica Peninsula, Table S1 in Supporting Information S1). While offsets from small earthquakes with proportionally small postseismic deformation (i.e., the 2018 event) are approximated by step functions, larger earthquakes with longer afterslip need to be dealt with carefully. To avoid contamination from the Nicoya and Jacó events, we limited our focus to southern Costa Rica, and excluded any stations located north of the CCRDB. From visual inspection, the resulting time series appear to be free of any remaining offsets or large common mode errors (Figure S1 in Supporting Information S1), though small signals may persist.

Our cleaned time series can then be fit to Equation 1.

$$y(t_i) = a + bt_i + A_1 \sin\left(2\pi t_i + \varphi_1\right) + A_2 \sin\left(4\pi t_i + \varphi_2\right) + \sum_{j=1}^{k} o_j H(t_i - T_j) + N_i \quad (1)$$

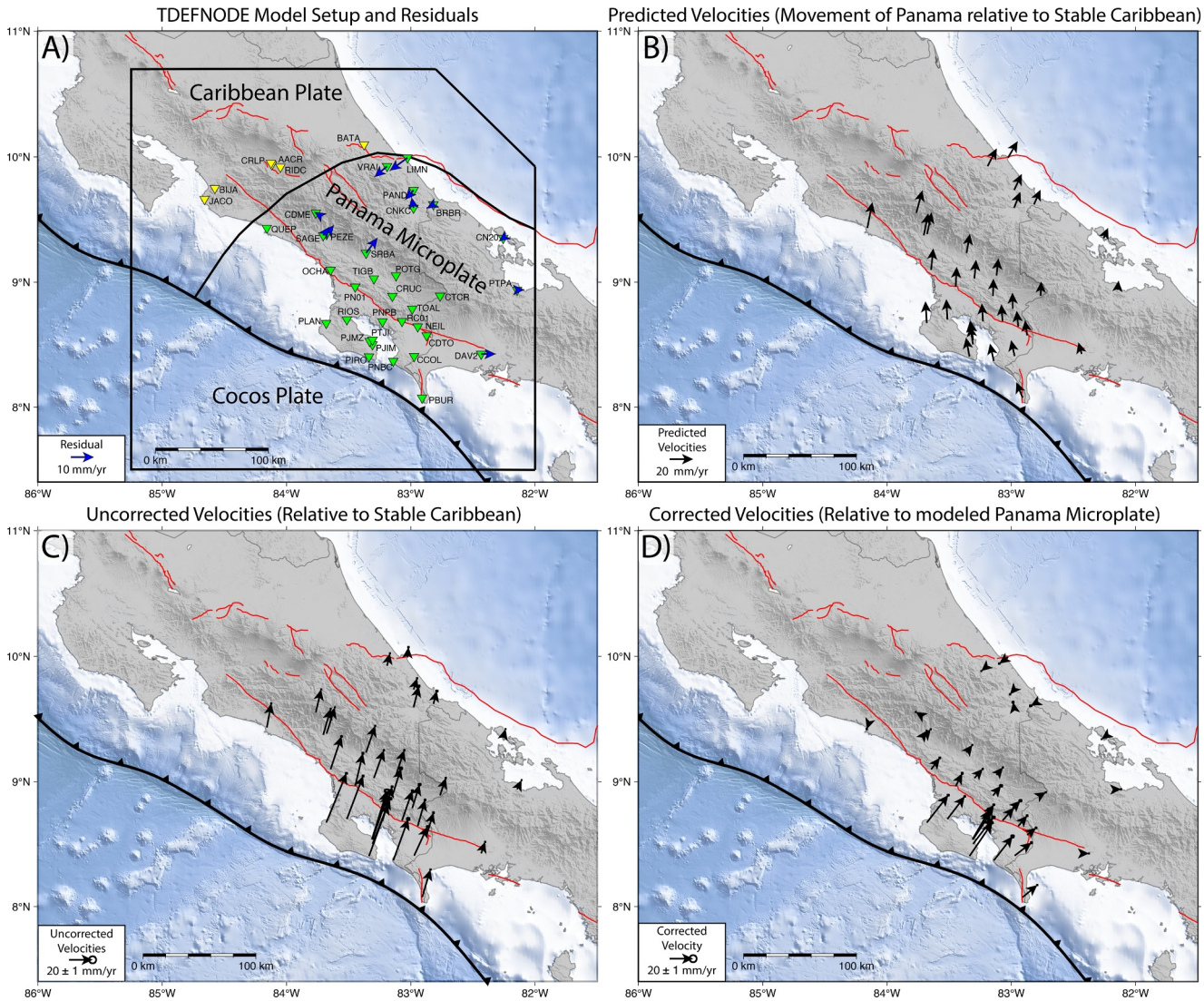

Figure 3. Overview of our block modeling and velocity correction. Panel (a) shows the setup of our block modeling. Block boundaries are shown as black lines. The continuation of the Middle American Trench outside of our block model is shown here, but not used in our model. All regional GNSS stations are plotted as colored triangles. All stations with blue arrows are used in block modeling and the blue arrows indicate residual velocity vectors, that is velocities relative to our modeled Panama plate. Green triangles indicate all stations used in our slip deficit inversion. Stations with yellow triangles are those within our region of study, but excluded from this study due to influences associated with the CCRDB. As we do not estimate the Euler pole of the Caribbean plate or the CCRDB, we do not use any velocity measurements of sites outside of the Panama Microplate. Panel (b) shows the predicted velocities of all stations from our block modeling, effectively showing the motion of our modeled Panama microplate relative to the Caribbean. Panel (c) shows the uncorrected inter-SSE velocities of all stations relative to the ITRF08 stable Caribbean (Altamimi et al., 2012). Panel (d) shows our corrected inter-SSE velocities that have our estimated Panama Microplate block motion removed, effectively showing velocities relative to our modeled Panama microplate. We note that the vector scale in (a) is double that in (b–d) in order to accentuate the differences in residual velocity estimates. In summary, the velocities shown in (d) are the velocities of (c) with (b) subtracted out.

Here, the first term (a) represents the initial position of each station. The second term (b) represents the velocity of a station (here, it is the inter-SSE velocity). The third and fourth terms represent a summation of harmonic modes of deformation where (A) represents the amplitude and (φ) represents a phase shift. As we only fit our time series with annual and semi-annual harmonics, we only include sinusoids of period 2π and 4π, respectively. The fifth term represents the summation of offsets from earthquakes, SSE, or equipment changes that are approximated as step functions of magnitude (o_j). Lastly the sixth term (N) represents the remaining noise in the time series. All parameters are simultaneously fit across the entire time series using least squares, such that the long-term velocity as well as the amplitude and phase shift of the sinusoid are the same across all offsets. While fitting our time series, data from either the day of an earthquake or from apparent transient signals (i.e. SSEs) were masked. Here,

we then used the best-fit *b* as our estimated inter-SSE velocity, with errors calculated from the covariance matrix (Table S2 in Supporting Information S1).

3.3. Block Modeling and Inter-SSE Velocity Correction

As the study area encompasses the western portion of the Panama microplate (e.g., Adamek et al., 1988), differential motion between the Panama microplate and the Caribbean plate must be accounted for to ensure that deformation on the NPDB does not influence our results. We accounted for differential motion between Panama and the Caribbean through a simple block-modeling approach using TDEFNODE (McCaffrey, 2009). The boundaries of the Panama microplate are defined by the CCRDB in the west, the NPDB to the north, the Middle American Trench to the south, and the edge of our study area in the east (Figure 3). To the north of the NPDB, we have the Caribbean plate, while the Cocos plate is south of the Middle American Trench (Figure 3). Although we included blocks other than the Panama microplate in our modeling, we did not estimate their poles of rotation but instead implemented the MORVEL-56 Euler poles (Argus et al., 2011).

While TDEFNODE can calculate coupling, we only used it to calculate the Euler poles of the Panama microplate relative to a stable Caribbean (Altamimi et al., 2012, Table 1), and the relative pole between the Panama microplate and the Cocos plate as defined in the MORVEL-56 model (Argus et al., 2011), and enforce free slip at all block boundaries. Additionally, to ensure that coupling does not influence the output Euler poles, we restricted sites used in TDEFNODE modeling to be those located far (≥100 km) from the Middle American Trench, those that show no discernible transient signals, and those having similar deformation rates to those located on Costa Rica's Caribbean coast (Figure 3). Additionally, in an effort to include as many data as possible, we downloaded time series for two sites outside of our network from the University of Nevada, Reno Geodetic Laboratory (DAV2, PTPA) (Blewitt et al., 2018) (http://geodesy.unr.edu/links.php), and added them to our block model. All input velocities were calculated using the method outlined in Section 3.2. Due to our exclusion of sites near the trench, this has the added benefit that inter-SSE velocities are the same as long-term velocities.

Using the Euler poles estimated in our block modeling, we corrected our calculated inter-SSE velocities to remove predicted relative motion between the Caribbean plate and the Panama microplate at all stations used in our inversions. To ensure that our results are reasonable, we also created a model where the inter-SSE velocities were corrected by removing the relative motion between the Caribbean plate and the Panama microplate as estimated in the MORVEL-56 angular velocities (Argus et al., 2011).

3.4. Modeling Approach

The resulting corrected inter-SSE velocities were then used to invert for the inter-SSE slip deficit rate on the Middle American megathrust using the code of Lindsey et al. (2021), under the back slip assumption (Savage, 1983), using the elastic Green's functions derived by Nikkhoo and Walter (2015) for triangular meshes. This code differs from standard elastic dislocation codes in that it can implement stress constraints that account for stress shadows updip of a fully coupled zone that may be frictionally unlocked yet remain kinematically coupled (Almeida et al., 2018), yielding more realistic inversion results. To determine the extent to which our model is influenced by these stress constraints, we also inverted our observations for an estimated slip deficit rate distribution that does not take these constraints into account (Figures S2 and S3 in Supporting Information S1). We used the Slab2.0 interface geometry (Hayes et al., 2018) that we shifted horizontally to better align with regional seismicity (Figures S4 and S5 in Supporting Information S1). This is the same base geometry of Perry et al. (2023), but with slight differences in fault discretization due to the use of a triangular mesh. We did not impose any additional boundary conditions for estimating the slip deficit rate in the stress-constrained inversion. In the non stress-constrained inversion, the bottom of the modeling domain is set to be freely creeping. Smoothing parameters for the models are selected based on L-curves of model misfit versus roughness (e.g., Chen et al., 2009; Du et al., 1992; Feng et al., 2012) (Figure S6 in Supporting Information S1). Model residuals are shown in Figure S7 of Supporting Information S1. We then tested the resolution limits of our model results by running checkerboard tests and assorted forward models to determine where we are likely to underestimate the slip deficit rate due to the GNSS network configuration (i.e., where offshore coupling is likely undetectable) (Figures 6 and 7). Additionally, we calculated the resolution spread of our model (Jónsson, 2002; Kyriakopoulos & Newman, 2016) to empirically determine regions where our results are poorly resolved. We note that the use of

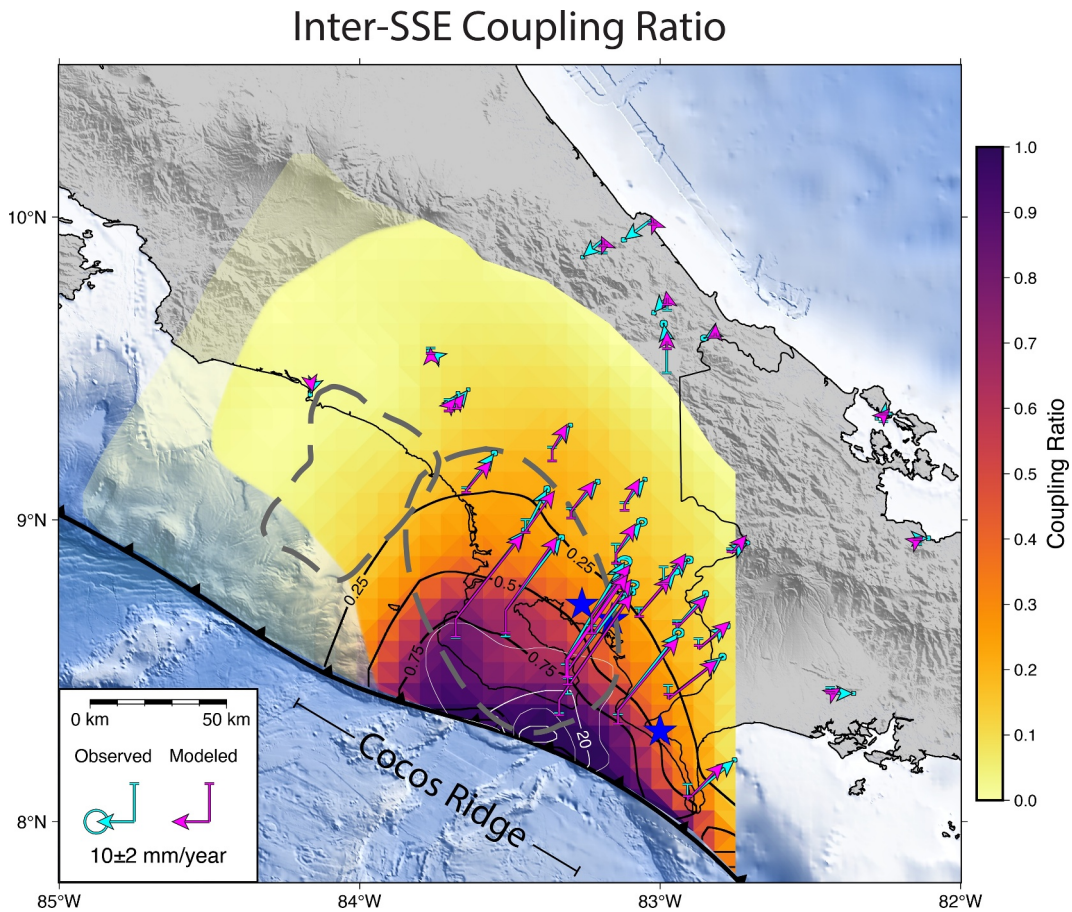

Figure 4. Map showing estimates of the inter-SSE coupling ratio for southern Costa Rica using stress-constrained models. Regions of resolution spread (Kyriakopoulos & Newman, 2016) lower than 40 km are set to be transparent. Epicenters of the three major historic $M > 7$ earthquakes are plotted as blue stars, while slip areas of the 1983 M_w 7.4 Osa event (Adamek et al., 1987) and the 1999 M_w 6.9 Quepos event (DeShon et al., 2003) are plotted in gray (on the right and left, respectively). Coupling contours (each contour is 0.25) are plotted as black lines. This figure shows the coupling estimate that has not had cumulative SSE slip removed. Cumulative SSE slip contours (each contour is 10 cm) from our re-modeled SSE slip inversions are plotted in white for reference. The largest coupling ratios occur in the region where slow slip has been observed and immediately surrounding this region.

checkerboard tests for probing the accuracy of models that account for stress shadows is not particularly informative, as checkerboard tests generally require inverting for physically unlikely coupling distributions.

To determine the effect SSE slip has on the calculated slip deficit, we re-modeled the four individual SSEs from Perry et al. (2023). We used the same code and slab geometry of our slip deficit inversions to ensure the various models are directly comparable (Figure S8 in Supporting Information S1). For the SSE inversions, we imposed the same boundary conditions of Perry et al. (2023), that is zero slip boundary conditions on the downdip and lateral edges of the modeling domain, and free slip at the trench. All four slip distributions are then combined into a time-averaged cumulative slip ($\bar{S}_c$, Equation 2):

$$\bar{S}_c = \frac{1}{n}\sum_{i=1}^{n}\frac{S_i}{t_{re}}, \text{where } S_i = \sum_{j=1}^{m} s_j \tag{2}$$

Here we refer to each group of SSEs that are clustered in time as an SSE episode with cumulative slip distribution S_i and recurrence interval t_{re}, where each individual SSE has the slip distribution s_j, and the number of slow slip episodes is n. In total, Perry et al. (2023) reported 5 individual events, one in 2013, two in 2018, and two in 2022, resulting in a recurrence interval of ~4.5 years. As the event in 2013 was only recorded by one station, there are

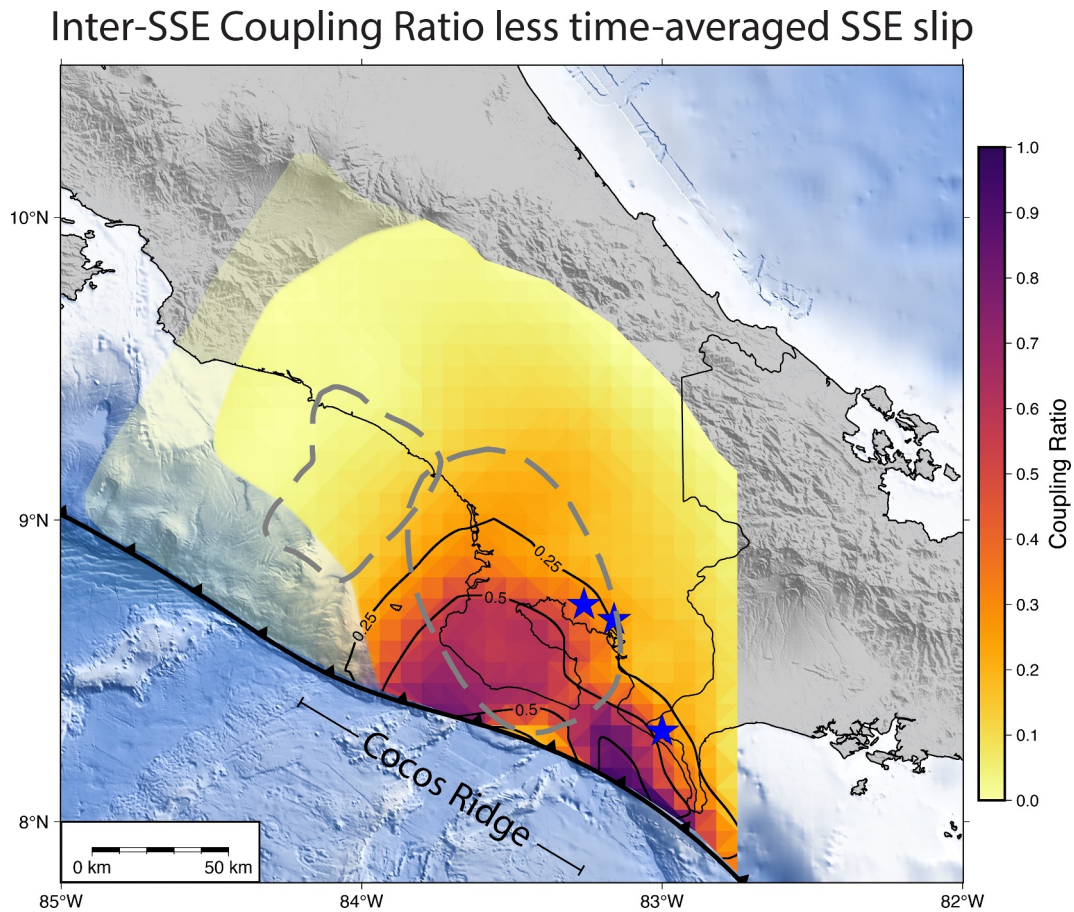

Figure 5. Map showing estimates of the inter-SSE coupling ratio for southern Costa Rica using stress-constrained models with time-averaged cumulative slow slip removed. Regions of resolution spread (Kyriakopoulos & Newman, 2016) lower than 40 km are set to be transparent. Epicenters of the three major historic $M > 7$ earthquakes are plotted as blue stars, while slip areas of the 1983 M_w 7.4 Osa event (Adamek et al., 1987) and the 1999 M_w 6.9 Quepos event (DeShon et al., 2003) are plotted in gray (on the right and left, respectively). Coupling contours (each contour is 0.25) are plotted as black lines. The largest coupling ratios occur in the region where slow slip has occurred and immediately surrounding this region. While significant decreases in coupling at the trench exist where slow slip has been observed (in comparison to Figure 4), a significant patch of high coupling exists within the slip region of the 1983 event.

only sufficient data for calculating the slip distribution of the two SSE episodes in 2018 and 2022. The resulting $\overline{S}_c$ was then subtracted from the calculated slip deficit rate giving us an SSE-corrected slip deficit rate. Finally, we converted from our estimated slip deficit rates to coupling ratio by dividing by the plate rate, as determined from the Cocos-Panama relative Euler pole from our block modeling (Figures 4 and 5, Table 1). This operates under the assumption that the observed SSEs including their slip distributions, slip magnitudes, and recurrence intervals are representative of the entire interseismic period, which may not be accurate. As such we present both the inter-SSE coupling estimates, and the modified coupling estimates (Figures 4 and 5, Figure S2 in Supporting Information S1).

Table 1
Euler Poles From Our Block Modeling Used in Velocity Corrections

Plate	Relative to	Longitude	Latitude	Omega (°/Myr)
CA-ITRF08	ITRF08	272.5787	31.3654	0.3543
Panama	CA-ITRF08	278.976	8.822	−3.633
Cocos	Panama	269.2296	12.5065	−4.2270

Note. The Panama Microplate Euler pole is defined relative to stable Caribbean of ITRF08 (Altamimi et al., 2012) (referred to as CA-ITRF08), while the Cocos Plate Euler pole is defined relative to the Panama microplate.

4. Results and Discussion

4.1. Coupling Estimates

Our estimates of both inter-SSE coupling and modified coupling with SSE slip removed are presented in Figures 4 and 5 for the stress-constrained case, and Figure S2 in Supporting Information S1 for the non-stress-constrained case. In our inter-SSE coupling maps, elevated coupling ratios exist

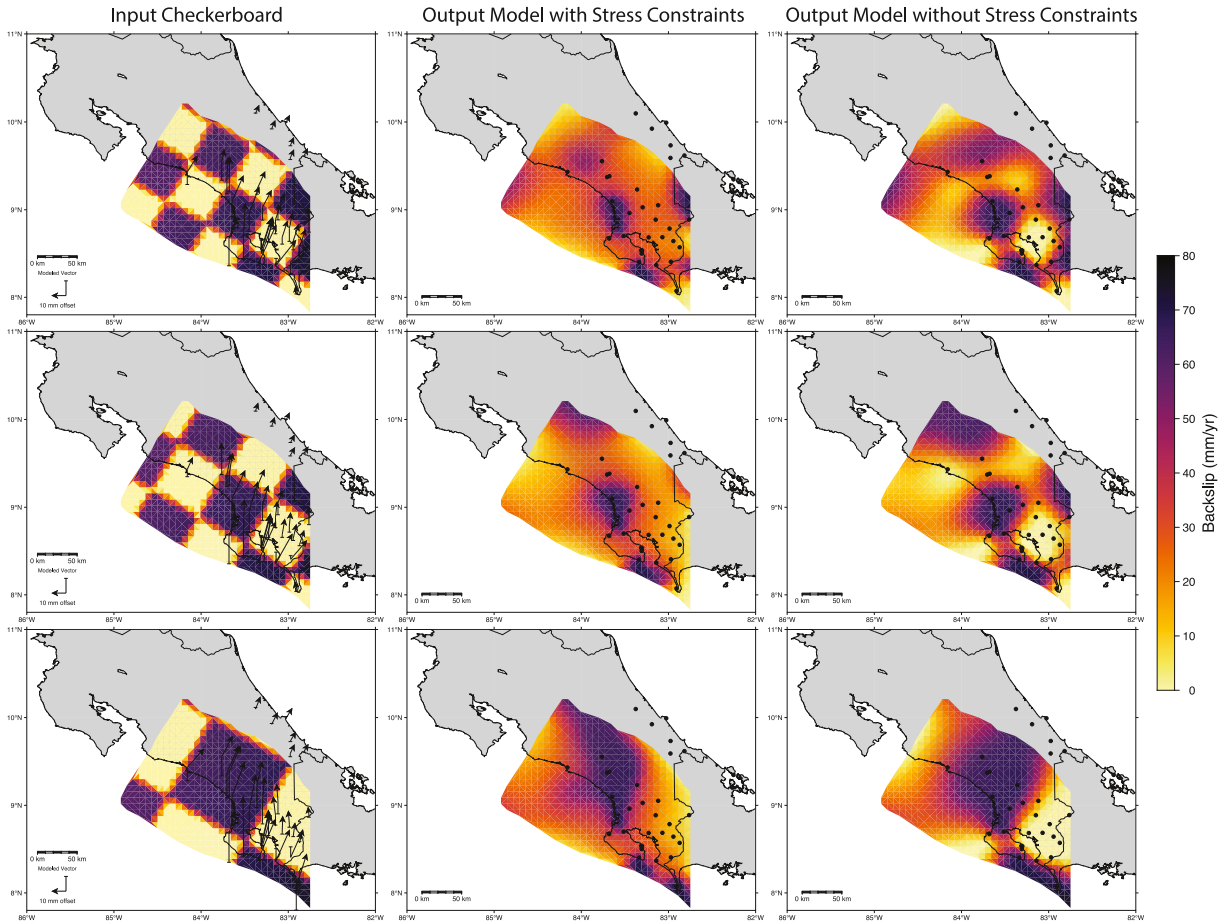

Figure 6. Checkerboard tests. The first column shows three different checkerboard tests with varying grid sizes, all displaying the input backslip, and the forward-modeled velocity vectors. The second column shows the inversion results from the stress constrained models, while the third column shows the results of the non-stress constrained models. Overall we see reasonable recovery of the checkerboard near the Osa peninsula, but significantly worse recovery in the region offshore in the west of our modeling domain, as is expected due to the lack of seafloor observations. We also note that the non-stress constrained model performs better in recovering the checkerboard, though this is expected as the stress-constrained models effectively penalize non-realistic slip distributions.

broadly mirroring the incident Cocos Ridge. While the region of highest coupling approaches 1.0 in the inter-SSE estimates, it largely coincides with the region of documented slow slip (Figure 4). Additionally, the spatial distribution of observed slow slip is smaller than the apparent coupled patch, indicating that significant coupling remains. In our coupling estimates with SSE-slip removed, the largest patch of elevated coupling is located beneath the Osa Peninsula with an estimated coupling ratio of ~0.5–0.7 (Figure 5), corresponding to an estimated slip deficit since the 1983 event of ~1.75–2 m (Figure S9 in Supporting Information S1). Near the epicentral region of the 1983 M_w 7.4 event (Adamek et al., 1987; Tajima & Kikuchi, 1995), the estimated coupling ratio decays to ~0.3–0.4 (Figures 4 and 5), corresponding with a slip deficit since the last major earthquake in the region of about ~1–1.25 m (Figure S9 in Supporting Information S1). In comparison, Adamek et al. (1987) estimated the average slip of the 1983 event to be 58 cm, which Tajima and Kikuchi (1995) suggested was underestimated.

In terms of the size of potential ruptures, estimates based on calculated slip deficit indicate that the region could produce an event of M_w ~7.4 (the same as the 1983 event) with ~30%–70% of accumulated slip deficit released, depending on the size of the rupture area. Based on our model results, the maximum moment release estimated within the region outlined in Adamek et al. (1987) would be equivalent with a M_w ~7.5 event (Figure S10 in Supporting Information S1), though a larger event is certainly possible given a larger slip area or the release of slip deficit accumulated prior to the 1983 event. In the same region, a release of only ~60% of estimated slip deficit could generate a M_w 7.4 event, while only a release of 20% of accumulated slip deficit would yield an event of M_w

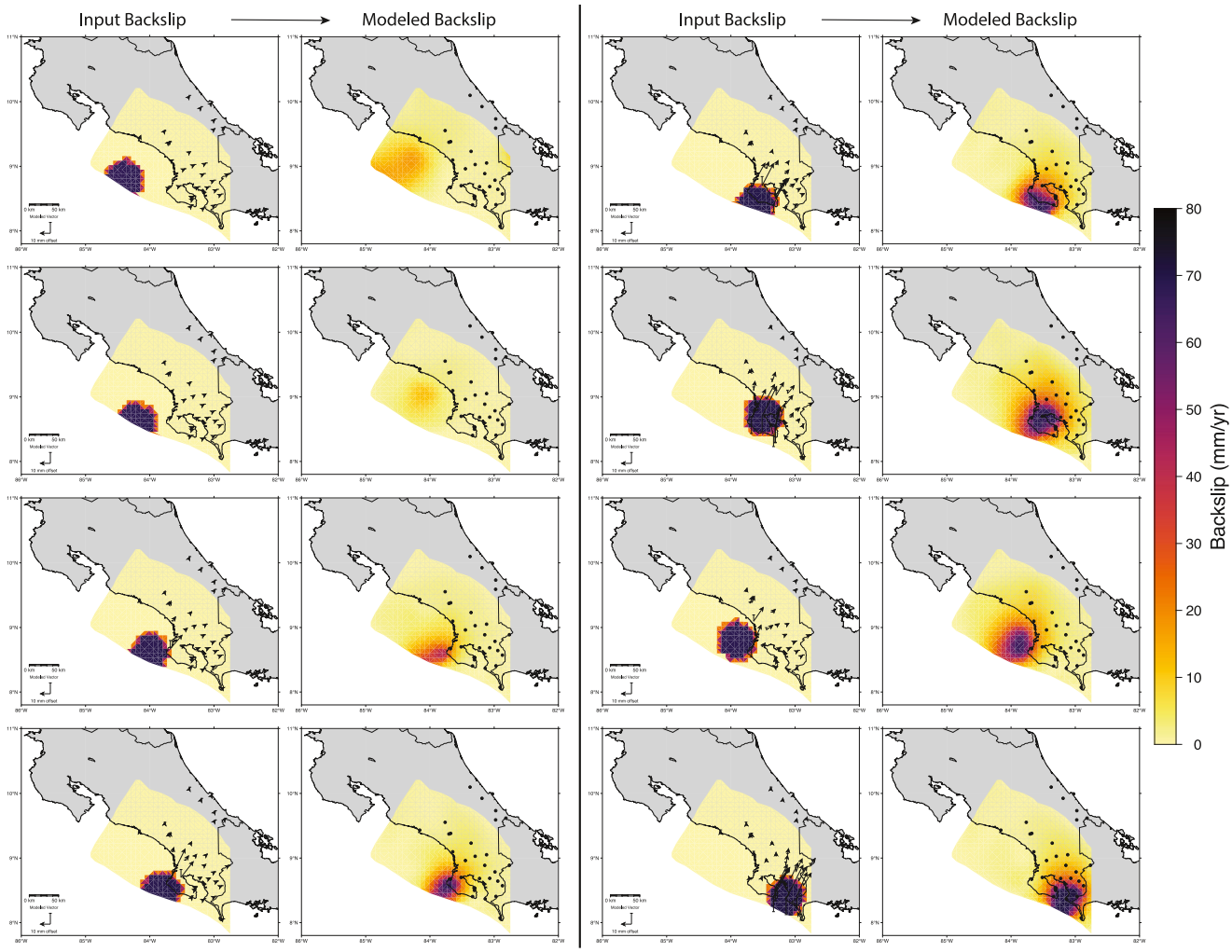

Figure 7. Suite of synthetic forward models to test the robustness of our stress constrained inversion. The first and third columns show and input backslip distribution, while the second and fourth columns show the output test stress constrained inversion using our GNSS network. Overall we see that coupling will be poorly recovered in the offshore area (southwestern portion of the modeling domain), and sometimes localized erroneously. In any case, coupling is well recovered at and immediately offshore the Osa peninsula.

~7.0 (Figure S10 in Supporting Information S1). Notably, to the southeast of the region of estimated slip in the 1983 event, we observe a strongly coupled patch in our modified coupling estimates that, if included in a future rupture, could increase the maximum estimated moment release to be equivalent with a M_w ~7.8 event (Figure S10 in Supporting Information S1). We do note that larger events are very much possible, as these estimates only account for slip deficit accumulation since the 1983 event.

While the overall pattern of coupling is similar in both the stress-constrained and unconstrained inversions (Figure S3 in Supporting Information S1), the use of elastic inversions that are stress constrained (e.g. Lindsey et al., 2021) imposes smoothing inherent to the method. As such, the coupling ratio appears subtly elevated in the unconstrained inversion, especially just offshore the Osa Peninsula. In the stress-constrained inversion, we find the coupling ratio decays to nearly zero between the western edge of the Osa Peninsula and the trace of the Quepos plateau and documented linear features in epicenter locations, as well as the region of rupture of the 1999 M_w 6.9 event (DeShon et al., 2003) (Figure 4). In the unconstrained inversion results, coupling extends further west to the region of the 1999 rupture (Figures S2 and S3 in Supporting Information S1). While model resolution in this region is limited, coupling near the Quepos plateau is expected to be largely concentrated on asperities that follow the trace of the plateau, usually interpreted as subducted seamounts, and comparatively low in surrounding regions (Bilek et al., 2003; Protti et al., 1995, 2001).

In comparison to previous coupling estimates of the region, we find some notable variation. Our estimated coupling ratio (without accounting for SSE slip) is generally less than that of Carvajal-Soto et al. (2020), though it matches reasonably well in the region of slow slip. In comparison to Kobayashi et al. (2014), our coupling estimates are generally higher, though we note that they also reported elevated coupling in the region of slow slip. In comparison to La Femina et al. (2009), we broadly see similar large-scale coupling ratios, but note that our model has higher spatial resolution in the study region.

4.2. Model Limitations

Our modeling of the Cocos-Panama coupling is dependent on an accurate representation of the block motion of the Panama microplate. Our exclusion of sites close to the trench serves to eliminate the influence of coupling on the estimated Euler pole of the Panama microplate. To explore potential variation in our coupling estimates, we also performed our same analysis using the MORVEL-56 estimated motion of the Panama microplate (Argus et al., 2011). While the general pattern in coupling is similar, the MORVEL-56-corrected model exhibits a significantly larger offshore coupled patch to the west of the Osa Peninsula in a region that is generally poorly constrained (Figure S11 in Supporting Information S1).

A combination of checkerboard resolution tests and synthetic forward models indicate that the region to the west of the Osa Peninsula, offshore of the Costa Rican mainland, is poorly resolved (Figures 6 and 7), with limited resolution of coupling more than ∼35 km from the coastline. Additionally, the far western edge of our modeling domain is also subject to limited resolution, though this is primarily due to a relatively sparse coastal network combined with the exclusion of sites within the CCRDB due to regional shearing (e.g., Carvajal-Soto et al., 2020; Marshall et al., 2000). By contrast, the region surrounding the Osa Peninsula from the trench to the Cordillera de Talamanca, encompassing estimated epicenters of historic large events, is well resolved.

One of the main benefits of using stress-constrained models is that by accounting for realistic stress distributions, they can more accurately estimate updip coupling given limited observations (Lindsey et al., 2021). However, the presence of near-trench observations on the Osa Peninsula limits the potential benefits of this method in this region, in that slip deficit on the shallow megathrust should already be well resolved. Additionally, imposing stress constraints in the inversion effectively nullifies the utility of the standard checkerboard tests, as these do not represent a physically realistic coupling distribution. While we present checkerboard tests in Figure 6, higher estimated performance of the non-stress constrained models is expected due to this issue.

Our method is also sensitive to selection of smoothing parameters for both coupling inversions and the SSE slip models. While we attempt to select optimal smoothing parameters in our coupling models (Figure S6 in Supporting Information S1), and the SSE slip models (Perry et al., 2023), this selection nonetheless can influence our results. Increased smoothing of our coupling estimates would remove any resolution of finer asperities that may be present and are supported by our observations, while lower smoothing would yield unreasonable and sharp transitions in coupling behavior. Arbitrarily high smoothing for the slow slip inversions would yield relatively low, but spatially uniform decrease in coupling ratios. By contrast lower smoothing would yield smaller patches with greater decreases in coupling. As our preferred model can account for the plate rate convergence in localized regions, lower smoothing in the slow slip models would likely yield negative coupling rations and is thus non-physical.

Another limitation is the degree to which our slow slip observations are predictably repeated throughout the interseismic period. To estimate the reduction in slip deficit and thus coupling from SSEs, we assume that the observed SSEs are representative of long-term behavior on the megathrust. While the observed episodes in 2018 and 2022 occurred in the same region, they exhibited some variation in both slip magnitude and spatial distribution. Peak slip in each SSE is generally ∼15 cm, with one event exhibiting up to 30 cm of slip (Perry et al., 2023). Additionally, observed slip distributions are generally localized downdip of the Cocos Ridge axial graben, though one event's slip distribution extends further to the northwest. Furthermore, with observations of only three distinct slow slip episodes, the estimated recurrence intervals could be significantly over or underestimated. Moreover, the same network-based pitfalls of our coupling estimate are also present in the estimation of SSE slip distributions, with limited resolution offshore and in regions with low station density (e.g., Perry et al., 2023), notably on the central southern coast of the Osa Peninsula and to the west of the peninsula. Nonetheless, in the last two slow slip episodes, the size and spatial distribution of slip is significant, and the potential influence on coupling should not be ignored.

4.3. Relationship to Slow Slip Events and Historical Seismicity

Our modified coupling estimates with time-averaged SSE slip removed exhibits similar patterns to our inter-SSE coupling models. In the regions both northwest and downdip of the peak of our observed slow slip, coupling ratios of ∼0.4–0.6 remain (Figure 5). The most significant decrease in estimated coupling occurs close to the trench where in some localized regions it is sufficient to fully account for the estimated inter-SSE coupling (e.g., Perry et al., 2023), while in the larger region of SSE slip the apparent release of strain by SSEs lowers the average coupling ratio by ∼0.2.

Dixon et al. (2014) showed that in the years preceding the 2012 M_w 7.6 Nicoya event, a number of SSEs occurred around the eventual rupture, effectively outlining the earthquake slip distribution, suggesting that at some locations SSEs may have some limited predictive power in delineating the spatial extent of future ruptures. Although the subducting bathymetry at the Osa Peninsula is more heterogeneous than at the Nicoya Peninsula to the north (Wang & Bilek, 2011, 2014), the observed SSEs at the Osa Peninsula occurred primarily in the same region, immediately down-dip of the Cocos Ridge axial graben (Perry et al., 2023), effectively limiting the predictive power that SSE slip distributions may have. While SSEs are often observed in conditionally stable regions surrounding seismogenic asperities (Bürgmann, 2018; Xie et al., 2020), we note that the presence of SSEs does not preclude the possibility of future seismic rupture on the same portion of the megathrust (e.g., Li & Gabriel, 2024). Regardless, future events may provide a test of the potential predictive ability of SSEs to delineate regions of eventual seismic rupture in this region.

Previous studies also have shown that SSEs can modulate stress distributions in the crust and may play a role in generating future seismic ruptures. Recent rate-and-state modeling of the interaction of SSEs and larger megathrust earthquakes has shown that SSEs can load nearby seismogenic asperities (Meng & Duan, 2022), effectively transferring stress from conditionally stable regions to frictionally locked asperities. Additionally, others have implied that transient stresses from SSEs can be large enough to trigger dynamic ruptures, though they are not a requirement for their occurrence (Li & Gabriel, 2024; Meng & Duan, 2022; Voss et al., 2018), and observations indicate SSEs have a limited role in directly triggering large earthquakes (Dascher-Cousineau & Bürgmann, 2024). Following this, while future SSEs at the Osa Peninsula should lower the overall slip deficit on the megathrust, whether they will play a role in either triggering or merely clock advancing the next rupture of the 1983 asperity remains an open question.

In comparison to the regions of estimated rupture for the 1983 event (Adamek et al., 1987; Tajima & Kikuchi, 1995), as well as epicenters of all known historical events (1983, 1941, and 1904), we find that the region of elevated coupling is largely coincident with the estimated earthquake slip distributions, extending updip from the epicenters of the two most recent historic events (Figures 4 and 5). Additionally, the limited seismic network coverage during the last event indicates that these estimates of both historic slip region and epicenters are relatively unconstrained.

The 1983 rupture has been documented as a relatively complex one, with low propagation speed and noted time-dependent variation in moment release (Adamek et al., 1987; Tajima & Kikuchi, 1995). This is largely attributed to heterogeneous frictional behavior linked to variable bathymetry, namely the combined influence of both the Cocos Ridge and the Cocos Ridge axial graben (Bilek et al., 2003). Given that the SSEs documented in Perry et al. (2023) seem to be linked to these same bathymetric features, it is possible that the region on the megathrust that hosts SSEs ruptured in the 1983 earthquake and may behave similarly in the future. On the other hand, regions of slow slip have been shown to act as persistent rupture barriers in Ecuador (Rolandone et al., 2018; Vaca et al., 2018), and a similar behavior here could limit the extent of a future seismic rupture.

5. Conclusions

We report a megathrust coupling model for the Middle American Trench offshore southern Costa Rica using new observations from continuous GNSS sites installed on and around the Osa Peninsula. Using these data and stress-constrained elastic inversions (Lindsey et al., 2021), we show a region of high coupling that is centered within the region thought to have slipped in the 1983 M_w 7.4 Osa earthquake (Adamek et al., 1987). Additionally, our estimated coupling ratio decays to nearly zero in the region of the 1999 M_w 6.9 Quepos event, though this may be due to the current observational network and lack of offshore resolution. Conservative estimates of slip deficit in the region of the 1983 event are sufficient to produce a similar or larger slip magnitude in a potential future event.

Additionally, we find significant coupling at the trench just offshore the Osa Peninsula. While the degree of coupling is reduced by the observed slip distributions of shallow SSEs (Perry et al., 2023), the effect of shallow SSEs on the overall state of coupling is concentrated in the uppermost portions of the megathrust. While this reduction of shallow coupling may mitigate the tsunamigenic potential of this region and Costa Rica's Pacific Coast has historically not experienced damaging tsunamis (e.g., Chacón-Barrantes & Protti, 2011), significant shallow coupling, and thus tsunami risk, remains. Nevertheless, as we are approaching the end of the ∼40-year recurrence interval (in fact, it has been 41 years since the 1983 event at the time of writing), these coupling estimates highlight significant seismic hazard for the region.

Data Availability Statement

GNSS data processing was completed using the GAMIT/GLOBK software suite (Herring, et al., 2015, 2018). All time series used in this study can be found in Muller and Perry (2024). Raw data from OVSICORI-operated sites are available through formal written requests to OVSICORI-UNA for joint collaborations. Similarly, raw data from IGN-operated sites must be requested from Álvaro A. Álvarez Calderón. Inverse modelling was done using the code of Lindsey et al. (2021). Input files, preferred coupling models, slow slip models, synthetic models, and associated scripts can be accessed through the data set, Perry et al. (2024). Figures 1 and 3–5, and Figures S2, S3, S5, S7, S8, S9, S11, and S12 in Supporting Information S1 were made using GMT (Wessel et al., 2019). Plots for Figure 2, and Figures S1, S4, S6, S10, S13, and S14 in Supporting Information S1 were made using python and the matplotlib library (Hunter, 2007; Van Rossum & Drake, 2009).

Acknowledgments
The authors would like to acknowledge Álvaro A. Álvarez Calderón from the Insituto Geografico Nacional (IGN) (https://gnss.rnp.go.cr/SBC/) and José Ana Gonzalez Carvajal from the Insituto Costarricense de Electricidad (ICE) for their work in collecting and providing GNSS data from stations they operate. Instrumentation and data from OVSICORI-UNA used in this research was supported by Costa Rican Emergency Law 8933 and by Universidad Nacional de Costa Rica through the project 0097–2020 "Sistema de monitoreo geodésico (SiMoGeod) de los volcanes y de la tectónica de Costa Rica." We acknowledge the huge work made by OVSICORI-UNA technical group to install and maintain the GNSS network. The authors would also like to thank Jeff Freymueller and an anonymous reviewer for helpful comments that greatly improved the manuscript. This work was supported by the National Research Foundation (NRF) of Singapore under its NRF Investigatorship Scheme (Award No. NRF-NRFI05-2019-0009 to EMH) and by the Singapore Ministry of Education (MOE) under the Tier 3b project "Integrating Volcano and Earthquake Science and Technology (InVEST)" (Award No. MOE-MOET32021-0002 to EMH and LF). This work comprises EOS contribution number 628.

References

Adamek, S., Frohlich, C., & Pennington, W. D. (1988). Seismicity of the Caribbean-Nazca boundary: Constraints on microplate tectonics of the Panama region. *Journal of Geophysical Research*, *93*(B3), 2053–2075. https://doi.org/10.1029/JB093iB03p02053

Adamek, S., Tajima, F., & Wiens, D. A. (1987). Seismic rupture associated with subduction of the Cocos Ridge. *Tectonics*, *6*(6), 757–774. https://doi.org/10.1029/TC006i006p00757

Almeida, R., Lindsey, E. O., Bradley, K., Hubbard, J., Mallick, R., & Hill, E. M. (2018). Can the updip limit of frictional locking on megathrusts be detected geodetically? Quantifying the effect of stress shadows on near-trench coupling. *Geophysical Research Letters*, *45*(10), 4754–4763. https://doi.org/10.1029/2018GL077785

Altamimi, Z., Métivier, L., & Collilieux, X. (2012). ITRF2008 plate motion model. *Journal of Geophysical Research*, *117*(B7). https://doi.org/10.1029/2011JB008930

Altamimi, Z., Rebischung, P., Métivier, L., & Collilieux, X. (2016). ITRF2014: A new release of the international terrestrial reference frame modeling nonlinear station motions. *Journal of Geophysical Research: Solid Earth*, *121*(8), 6109–6131. https://doi.org/10.1002/2016JB013098

Ambraseys, N. N., & Adams, R. D. (1996). Large-magnitude central American earthquakes, 1898–1994. *Geophysical Journal International*, *127*(3), 665–692. https://doi.org/10.1111/j.1365-246X.1996.tb04046.x

Argus, D. F., Gordon, R. G., & DeMets, C. (2011). Geologically current motion of 56 plates relative to the no-net-rotation reference frame: NNR-MORVEL56. *Geochemistry, Geophysics, Geosystems*, *12*(11). https://doi.org/10.1029/2011GC003751

Bilek, S. L., Schwartz, S. Y., & DeShon, H. R. (2003). Control of seafloor roughness on earthquake rupture behavior. *Geology*, *31*(5), 455. https://doi.org/10.1130/0091-7613(2003)031<0455:COSROE>2.0.CO;2

Blewitt, G., Hammond, W., & Kreemer, C. (2018). Harnessing the GPS data explosion for interdisciplinary science. *Eos*, *99*. https://doi.org/10.1029/2018EO104623

Boehm, J., Werl, B., & Schuh, H. (2006). Troposphere mapping functions for GPS and very long baseline interferometry from European Centre for Medium-Range Weather Forecasts operational analysis data: Troposphere mapping functions from ECMWF. *Journal of Geophysical Research*, *111*(B2). https://doi.org/10.1029/2005JB003629

Brown, K., Tryon, M., Deshon, H., Dorman, L., & Schwartz, S. (2005). Correlated transient fluid pulsing and seismic tremor in the Costa Rica subduction zone. *Earth and Planetary Science Letters*, *238*(1–2), 189–203. https://doi.org/10.1016/j.epsl.2005.06.055

Bürgmann, R. (2018). The geophysics, geology and mechanics of slow fault slip. *Earth and Planetary Science Letters*, *495*, 112–134. https://doi.org/10.1016/j.epsl.2018.04.062

Camacho, E., Hutton, W., & Pacheco, J. F. (2010). A new look at evidence for a Wadati-Benioff zone and active convergence at the North Panama deformed belt. *Bulletin of the Seismological Society of America*, *100*(1), 343–348. https://doi.org/10.1785/0120090204

Carvajal-Soto, L. A., Ito, T., Protti, M., & Kimura, H. (2020). Earthquake potential in Costa Rica using three scenarios for the central Costa Rica deformed belt as western boundary of the Panama microplate. *Journal of South American Earth Sciences*, *97*, 102375. https://doi.org/10.1016/j.jsames.2019.102375

Chacón-Barrantes, S. E., & Protti, M. (2011). Modeling a tsunami from the Nicoya, Costa Rica, seismic gap and its potential impact in Puntarenas. *Journal of South American Earth Sciences*, *31*(4), 372–382. https://doi.org/10.1016/j.jsames.2011.03.013

Chen, T., Newman, A. V., Feng, L., & Fritz, H. M. (2009). Slip distribution from the 1 April 2007 Solomon Islands earthquake: A unique image of near-trench rupture. *Geophysical Research Letters*, *36*(16), L16307. https://doi.org/10.1029/2009GL039496

Dascher-Cousineau, K., & Bürgmann, R. (2024). Global subduction slow slip events and associated earthquakes. *Science Advances*, *10*(35), eado2191. https://doi.org/10.1126/sciadv.ado2191

Davis, E. E., Villinger, H., & Sun, T. (2015). Slow and delayed deformation and uplift of the outermost subduction prism following ETS and seismogenic slip events beneath Nicoya Peninsula, Costa Rica. *Earth and Planetary Science Letters*, *410*, 117–127. https://doi.org/10.1016/j.epsl.2014.11.015

DeMets, C., Gordon, R. G., & Argus, D. F. (2010). Geologically current plate motions. *Geophysical Journal International*, *181*(1), 1–80. https://doi.org/10.1111/j.1365-246X.2009.04491.x

DeShon, H. R., Schwartz, S. Y., Bilek, S. L., Dorman, L. M., Gonzalez, V., Protti, J. M., et al. (2003). Seismogenic zone structure of the southern Middle America Trench, Costa Rica. *Journal of Geophysical Research*, *108*(B10), 2002JB002294. https://doi.org/10.1029/2002JB002294

Dill, R., & Dobslaw, H. (2013). Numerical simulations of global-scale high-resolution hydrological crustal deformations: High-resolution hydrological loading. *Journal of Geophysical Research: Solid Earth*, *118*(9), 5008–5017. https://doi.org/10.1002/jgrb.50353

Dixon, T. H., Jiang, Y., Malservisi, R., McCaffrey, R., Voss, N., Protti, M., & Gonzalez, V. (2014). Earthquake and tsunami forecasts: Relation of slow slip events to subsequent earthquake rupture. *Proceedings of the National Academy of Sciences*, *111*(48), 17039–17044. https://doi.org/10.1073/pnas.1412299111

Du, Y., Aydin, A., & Segall, P. (1992). Comparison of various inversion techniques as applied to the determination of a geophysical deformation model for the 1983 Borah Peak earthquake. *Bulletin of the Seismological Society of America*, *82*(4), 1840–1866. https://doi.org/10.1785/BSSA0820041840

Dziewonski, A. M., Chou, T. A., & Woodhouse, J. H. (1981). Determination of earthquake source parameters from waveform data for studies of global and regional seismicity. *Journal of Geophysical Research*, *86*(B4), 2825–2852. https://doi.org/10.1029/JB086iB04p02825

Ekström, G., Nettles, M., & Dziewoński, A. M. (2012). The global CMT project 2004–2010: Centroid-moment tensors for 13,017 earthquakes. *Physics of the Earth and Planetary Interiors*, *200–201*, 1–9. https://doi.org/10.1016/j.pepi.2012.04.002

Feng, L., Newman, A. V., Protti, M., González, V., Jiang, Y., & Dixon, T. H. (2012). Active deformation near the Nicoya Peninsula, northwestern Costa Rica, between 1996 and 2010: Interseismic megathrust coupling: Nicoya interseismic megathrust coupling. *Journal of Geophysical Research*, *117*(B6). https://doi.org/10.1029/2012JB009230

Hayes, G. P., Moore, G. L., Portner, D. E., Hearne, M., Flamme, H., Furtney, M., & Smoczyk, G. M. (2018). SLAB2, a comprehensive subduction zone geometry model. *Science*, *362*(6410), 58–61. https://doi.org/10.1126/science.aat4723

Herring, T. A., Floyd, M. A., King, R. W., & McClusky, S. C. (2015). GLOBK reference manual: Global Kalman filter VLBI and GPS analysis program release (Vol. *10*).6.

Herring, T. A., King, R. W., Floyd, M. A., & McClusky, S. C. (2018). GAMIT reference manual: GPS analysis at MIT.

Herring, T. A., Melbourne, T. I., Murray, M. H., Floyd, M. A., Szeliga, W. M., King, R. W., et al. (2016). Plate boundary observatory and related networks: GPS data analysis methods and geodetic products. *Reviews of Geophysics*, *54*(4), 759–808. https://doi.org/10.1002/2016RG000529

Hobbs, T. E., Kyriakopoulos, C., Newman, A. V., Protti, M., & Yao, D. (2017). Large and primarily updip after-slip following the 2012 Mw 7.6 Nicoya, Costa Rica, earthquake. *Journal of Geophysical Research: Solid Earth*, *122*(7), 5712–5728. https://doi.org/10.1002/2017JB014035

Hunter, J. D. (2007). Matplotlib: A 2D graphics environment. *Computing in Science and Engineering*, *9*(3), 90–95. https://doi.org/10.1109/MCSE.2007.55

Iinuma, T., Protti, M., Obana, K., González, V., Van der Laat, R., Kato, T., et al. (2004). Inter-plate coupling in the Nicoya Peninsula, Costa Rica, as deduced from a trans-peninsula GPS experiment. *Earth and Planetary Science Letters*, *223*(1–2), 203–212. https://doi.org/10.1016/j.epsl.2004.04.016

Jiang, Y., Wdowinski, S., Dixon, T. H., Hackl, M., Protti, M., & Gonzalez, V. (2012). Slow slip events in Costa Rica detected by continuous GPS observations, 2002–2011. *Geochemistry, Geophysics, Geosystems*, *13*(4). https://doi.org/10.1029/2012GC004058

Jónsson, S. (2002). Fault slip distribution of the 1999 Mw 7.1 Hector mine, California, earthquake, estimated from satellite radar and GPS measurements. *Bulletin of the Seismological Society of America*, *92*(4), 1377–1389. https://doi.org/10.1785/0120000922

Kato, A., Obara, K., Igarashi, T., Tsuruoka, H., Nakagawa, S., & Hirata, N. (2012). Propagation of slow slip leading up to the 2011 M_w 9.0 Tohoku-Oki earthquake. *Science*, *335*(6069), 705–708. https://doi.org/10.1126/science.1215141

Kellogg, J. N., Vega, V., Stailings, T. C., Aiken, C. L. V., & Kellogg, J. N. (1995). Tectonic development of Panama, Costa Rica, and the Colombian Andes: Constraints from global positioning system geodetic studies and gravity. In *Geological society of America special papers* (Vol. 295, pp. 75–90). Geological Society of America. https://doi.org/10.1130/SPE295-p75

Kobayashi, D., La Femina, P., Geirsson, H., Chichaco, E., Abrego, A. A., Mora, H., & Camacho, E. (2014). Kinematics of the western Caribbean: Collision of the Cocos Ridge and upper plate deformation. *Geochemistry, Geophysics, Geosystems*, *15*(5), 1671–1683. https://doi.org/10.1002/2014GC005234

Kyriakopoulos, C., & Newman, A. V. (2016). Structural asperity focusing locking and earthquake slip along the Nicoya Megathrust, Costa Rica. *Journal of Geophysical Research: Solid Earth*, *121*(7), 5461–5476. https://doi.org/10.1002/2016JB012886

La Femina, P., Dixon, T. H., Govers, R., Norabuena, E., Turner, H., Saballos, A., et al. (2009). Fore-arc motion and Cocos Ridge collision in Central America. *Geochemistry, Geophysics, Geosystems*, *10*(5). https://doi.org/10.1029/2008GC002181

Li, D., & Gabriel, A. (2024). Linking 3D long-term slow-slip cycle models with rupture dynamics: The Nucleation of the 2014 M_w 7.3 Guerrero, Mexico earthquake. *AGU Advances*, *5*(2), e2023AV000979. https://doi.org/10.1029/2023AV000979

Lindsey, E. O., Mallick, R., Hubbard, J. A., Bradley, K. E., Almeida, R. V., Moore, J. D. P., et al. (2021). Slip rate deficit and earthquake potential on shallow megathrusts. *Nature Geoscience*, *14*(5), 321–326. https://doi.org/10.1038/s41561-021-00736-x

Lundgren, P., Protti, M., Donnellan, A., Heflin, M., Hernandez, E., & Jefferson, D. (1999). Seismic cycle and plate margin deformation in Costa Rica: GPS observations from 1994 to 1997. *Journal of Geophysical Research*, *104*(B12), 28915–28926. https://doi.org/10.1029/1999JB900283

Malservisi, R., Schwartz, S. Y., Voss, N., Protti, M., Gonzalez, V., Dixon, T. H., et al. (2015). Multiscale postseismic behavior on a megathrust: The 2012 Nicoya earthquake, Costa Rica. *Geochemistry, Geophysics, Geosystems*, *16*(6), 1848–1864. https://doi.org/10.1002/2015GC005794

Marshall, J. S., Fisher, D. M., & Gardner, T. W. (2000). Central Costa Rica deformed belt: Kinematics of diffuse faulting across the western Panama block. *Tectonics*, *19*(3), 468–492. https://doi.org/10.1029/1999tc001136

Maubant, L., Frank, W. B., Wallace, L. M., Williams, C. A., & Hamling, I. (2023). Imaging the spatiotemporal evolution of plate coupling with Interferometric Radar (InSAR) in the Hikurangi subduction zone. *Geophysical Research Letters*, *50*(19), e2023GL105388. https://doi.org/10.1029/2023GL105388

Maubant, L., Radiguet, M., Pathier, E., Doin, M., Cotte, N., Kazachkina, E., & Kostoglodov, V. (2022). Interseismic coupling along the Mexican subduction zone seen by InSAR and GNSS. *Earth and Planetary Science Letters*, *586*, 117534. https://doi.org/10.1016/j.epsl.2022.117534

McCaffrey, R. (2009). Time-dependent inversion of three-component continuous GPS for steady and transient sources in northern Cascadia. *Geophysical Research Letters*, *36*(7), 2008GL036784. https://doi.org/10.1029/2008GL036784

Meng, Q., & Duan, B. (2022). Dynamic modeling of interactions between shallow slow-slip events and subduction earthquakes. *Seismological Research Letters*, *XX*, 1–11. https://doi.org/10.1785/0220220138

Molnar, P., & Sykes, L. R. (1969). Tectonics of the Caribbean and Middle America regions from focal mechanisms and seismicity. *Geological Society of America Bulletin*, *80*(9), 1639. https://doi.org/10.1130/0016-7606(1969)80[1639:TOTCAM]2.0.CO;2

Morell, K. D., Fisher, D. M., & Gardner, T. W. (2008). Inner forearc response to subduction of the Panama Fracture Zone, southern Central America. *Earth and Planetary Science Letters*, *265*(1–2), 82–95. https://doi.org/10.1016/j.epsl.2007.09.039

Muller, C., & Perry, M. (2024). Interseismic megathrust coupling at the Osa Peninsula, Costa Rica [Dataset]. *Zenodo*. https://doi.org/10.5281/zenodo.14009227

Nikkhoo, M., & Walter, T. R. (2015). Triangular dislocation: An analytical, artefact-free solution. *Geophysical Journal International*, *201*(2), 1119–1141. https://doi.org/10.1093/gji/ggv035

Perry, M., Muller, C., Protti, M., Feng, L., & Hill, E. M. (2023). Shallow slow slip events identified offshore the Osa peninsula in southern Costa Rica from GNSS time series. *Geophysical Research Letters*, *50*(20), e2023GL104771. https://doi.org/10.1029/2023GL104771

Perry, M., Muller, C., Protti, M., Lujia, F., & Hill, E. (2024). Replication data for: Interseismic megathrust coupling at the Osa Peninsula, Costa Rica (version 2) [Dataset]. *DR-NTU (Data)*. https://doi.org/10.21979/N9/XWBEKD

Protti, M., González, V., Newman, A. V., Dixon, T. H., Schwartz, S. Y., Marshall, J. S., et al. (2014). Nicoya earthquake rupture anticipated by geodetic measurement of the locked plate interface. *Nature Geoscience*, *7*(2), 117–121. https://doi.org/10.1038/ngeo2038

Protti, M., Güendel, F., & Malavassi, E. (2001). *Evaluación del Potencial Sísmico de la Península de Nicoya*. Editorial Fundación UNA, 1ra. edición, 144.

Protti, M., McNally, K., Pacheco, J., González, V., Montero, C., Segura, J., et al. (1995). The March 25, 1990 ($M_w = 7.0$, $M_L = 6.8$), earthquake at the entrance of the Nicoya Gulf, Costa Rica: Its prior activity, foreshocks, aftershocks, and triggered seismicity. *Journal of Geophysical Research*, *100*(B10), 20345–20358. https://doi.org/10.1029/94JB03099

Protti, M., & Schwartz, S. Y. (1994). Mechanics of back arc deformation in Costa Rica: Evidence from an aftershock study of the April 22, 1991, Valle de la Estrella, Costa Rica, earthquake (M_w =7.7). *Tectonics*, *13*(5), 1093–1107. https://doi.org/10.1029/94TC01319

Rodriguez, M., DeMets, C., Rogers, R., Tenorio, C., & Hernandez, D. (2009). A GPS and modelling study of deformation in northern Central America. *Geophysical Journal International*, *178*(3), 1733–1754. https://doi.org/10.1111/j.1365-246X.2009.04251.x

Rolandone, F., Nocquet, J.-M., Mothes, P. A., Jarrin, P., Vallée, M., Cubas, N., et al. (2018). Areas prone to slow slip events impede earthquake rupture propagation and promote afterslip. *Science Advances*, *4*(1), eaao6596. https://doi.org/10.1126/sciadv.aao6596

Savage, J. C. (1983). A dislocation model of strain accumulation and release at a subduction zone. *Journal of Geophysical Research*, *88*(B6), 4984–4996. https://doi.org/10.1029/JB088iB06p04984

Styron, R., García-Pelaez, J., & Pagani, M. (2020). CCAF-DB: The Caribbean and Central American active Fault database. *Natural Hazards and Earth System Sciences*, *20*(3), 831–857. https://doi.org/10.5194/nhess-20-831-2020

Suárez, G., Pardo, M., Domínguez, J., Ponce, L., Montero, W., Boschini, I., & Rojas, W. (1995). The Limón, Costa Rica earthquake of April 22, 1991: Back arc thrusting and collisional tectonics in a subduction environment. *Tectonics*, *14*(2), 518–530. https://doi.org/10.1029/94TC02546

Tajima, F., & Kikuchi, M. (1995). Tectonic implications of the seismic ruptures associated with the 1983 and 1991 Costa Rica earthquakes. In *Geological society of America special papers* (Vol. 295, pp. 327–340). Geological Society of America. https://doi.org/10.1130/SPE295-p327

Uchida, N., Iinuma, T., Nadeau, R. M., Bürgmann, R., & Hino, R. (2016). Periodic slow slip triggers megathrust zone earthquakes in northeastern Japan. *Science*, *351*(6272), 488–492. https://doi.org/10.1126/science.aad3108

Vaca, S., Vallée, M., Nocquet, J.-M., Battaglia, J., & Régnier, M. (2018). Recurrent slow slip events as a barrier to the northward rupture propagation of the 2016 Pedernales earthquake (Central Ecuador). *Tectonophysics*, *724–725*, 80–92. https://doi.org/10.1016/j.tecto.2017.12.012

Van Rossum, G., & Drake, F. L. (2009). Python 3 reference manual. Create Space.

Voss, N., Dixon, T. H., Liu, Z., Malservisi, R., Protti, M., & Schwartz, S. (2018). Do slow slip events trigger large and great megathrust earthquakes? *Science Advances*, *4*(10), eaat8472. https://doi.org/10.1126/sciadv.aat8472

Wang, K., & Bilek, S. L. (2011). Do subducting seamounts generate or stop large earthquakes? *Geology*, *39*(9), 819–822. https://doi.org/10.1130/G31856.1

Wang, K., & Bilek, S. L. (2014). Invited review paper: Fault creep caused by subduction of rough seafloor relief. *Tectonophysics*, *610*, 1–24. https://doi.org/10.1016/j.tecto.2013.11.024

Wessel, P., Luis, J. F., Uieda, L., Scharroo, R., Wobbe, F., Smith, W. H. F., & Tian, D. (2019). The generic mapping tools version 6. *Geochemistry, Geophysics, Geosystems*, *20*(11), 5556–5564. https://doi.org/10.1029/2019GC008515

Xie, S., Dixon, T. H., Malservisi, R., Jiang, Y., Protti, M., & Muller, C. (2020). Slow slip and inter-transient locking on the Nicoya megathrust in the late and early stages of an earthquake cycle. *Journal of Geophysical Research: Solid Earth*, *125*(11), e2020JB020503. https://doi.org/10.1029/2020JB020503

Erratum

The originally published version of this article contained an error. The tenth sentence of the first paragraph of Section 3.4 has been corrected to the following: "We then tested the resolution limits of our model results by running checkerboard tests and assorted forward models to determine where we are likely to underestimate the slip deficit rate due to the GNSS network configuration (i.e., where offshore coupling is likely undetectable) (Figures 6 and 7)." This may be considered the authoritative version of record.